Penerbit Akademia Baru

CFD Letters
AN INTERNATIONAL JOURNAL
Editor-in-Chief
Khalid M. Saqr

Transition Thresholds and Routes to Unsteadiness of Magneto-Convective Flows in Tall Cavities at Low-Prandtl-Number Fluids

Open Access

Ridha Djebali[1,*], Said Abboudi[2] and Mohamed Ammar Abbassi[3]

[1] Laboratory of Subatomic Physics, Nanosciences and Energetics, IPEST, University of Carthage, Tunisia
[2] ICB UMR 6303, CNRS, Université de Bourgogne Franche-Comté, UTBM Département COMM, F-90010, Belfort, France
[3] UR: Matériaux, Energie et Energies Renouvelables (MEER), Université de Gafsa, Tunisie

ARTICLE INFO

ABSTRACT

The present study aims to investigate numerically the routes to unsteadiness behavior inside tall cavities at low Prandtl numbers (Pr=0.01-0.1) under imposed horizontal magnetic field. The transition thresholds are marked under the variation of the cavity aspect ratio Ar=W/H (1/8, 1/4, 1/2), the Rayleigh number Ra (10^4-5×10^7) and the Hartmann number Ha (0-150). The Lattice Boltzmann (LBM) approach is used to solve the governing equations. Horizontal temperature gradient is responsible of the convective motion and heat transfer. The changes in the convective flow patterns and temperature contours due to the effects of varying the controlling parameters and associated heat transfer are examined. It has been concluded that the flow is strongly unstable and presents multi-cellular structure at Pr=0.01 typical of liquid metal compared to Pr=0.1 cases. The same effect is observed by decreasing the cavity aspect ratio Ar. The Magnetic field magnitude necessary to control and stabilize the flow is the weaker for Pr=0.1. Increasing gradually the Rayleigh number Ra, the flow undergoes transition to steady state with fewer cells than at low Ra. the transition occurs at a threshold value showing weak growth rate in the Ha_{cr} compared to Ra variation. Increasing the Prandtl number to 0.1, the core flow structure is distorted due to the Lorentz forces which outweigh the buoyancy forces and a thermal stratification is clearly established. For high Hartman numbers and Rayleigh numbers, the stretching effects suppress the unsteady behaviour and results in steady state with extended unicellular pattern in the direction of Lorentz force.

Keywords:
Lattice Boltzmann method, low Prandtl numbers, routes to unsteadiness, flow patterns, Transition thresholds, multi-cellular structure, thermal stratification

[*] Corresponding author.
E-mail address: jbelii_r@hotmail.fr or Ridha.djebali@ipein.rnu.tn (Ridha Djebali)

1. Introduction

Lorentz force due to externally imposed in computational fluid dynamics, denoted as MHD, is used for the control in a wide ranges engineering problem and scientific researches [1-9]. The MHD control is used, among others purposes, for flow stabilization. At certain values of the flow monitoring parameters (critical values known as transition thresholds), the control is Lorentz force is used to suppress the arising oscillatory instabilities.

MHD control idea was first employed in Hurle experiments [10] and has been used after in several technological processes such as processing of semiconductor monocrystals. Besides, a growing interest in studying the convective behavior of low Prandtl number fluids as characteristic of liquid metal flows in melting / solidification enclosures. Such cases are devoted to academic purposes and are considered as research useful configurations for codes test and benchmarking since exhibiting very strong and complex nonlinear behavior [11-12].

Djebali *et al.,* [13] conducted a 2D analysis of MHD Convective Heat Transfer in Saturated Porous Square Enclosure using the LB method. The effects of the Rayleigh number, Hartmann number, Darcy number (Da) and the medium inclination angle from the horizontal, the magnetic field orientation and the medium porosity are investigated in wide ranges encountered in industrial and engineering applications. It has been concluded that the flow and thermal patterns depend strongly on Ra and Da parameter and the cavity tilting. However, for low Ha it depends marginally on the medium porosity. At high Ha values, a suppression of the convective currents and a great reduction of heat transfer rate are noticed.

Djebali *et al.,* [14] performed a study on unsteady 2D MHD natural convection flow of electrically conducting fluid in a square cavity for moderate Ra and for 0.01≤Pr≤10, 0≤Ha≤100 and and a magnetic field tilting angle ranging from 0° to 90°. It has been observed that for Ra≥105 without magnetic field and low Pr values, the flow is unsteady multicellular. While, increasing progressively Pr, the flow experiences a transition to steady bi-cellular, the transition occurs at critical value Pr≤ 0.1. For Pr≥0.1, the viscous forces outweigh the buoyancy forces and the flow structure is distorted leading to a thermal stratification. Besides, high magnetic field damps the unsteady behaviour and leads to an extended unicellular pattern.

Sathiyamoorthy and Chamkha [15] used a penalty finite elements method with bi-quadratic rectangular elements to study the 2D MHD natural convection and heat transfer within a square enclosure for Pr=0.054, Ra=10^5, 0≤Ha≤100, different field inclinations and different thermal boundary conditions. It has been concluded that the local heat transfer at the floor revealed oscillatory behavior for both case of thermal boundary conditions. Moreover, it has been shown that the heat transfer decreases distinctly by increasing the Ha number.

Yu *et al.,* [16] studied the MHD natural convection flows with different field inclinations in rectangular cavities using a second-order compact finite difference algorithm. Calculations are performed in a wide range of Ra number and Ha number at the Prandtl number Pr = 0.025. It has been observed that the Nusselt number is determined by the strength of the magnetic field and its inclination particularly for cavity low aspect ratios. It has been demonstrated also that the maximum non-dimensional component parallel to the magnetic field varies as $u_{max}^{//} \sim \text{Ra} \times \text{Ha}^{-1.5}$ and the component perpendicular to the magnetic field varies as $u_{max}^{\perp} \sim \text{Ra} \times \text{Ha}^{-2}$.

Ganaoui and Djebali [17] used the LBM to evaluate transitional thresholds for low Prandtl number flows in enclosures. The horizontal and vertical Bridgmann cavities are considered. The emerging results were in good agreement with very accurate literature benchmarks.

Han [18] investigated the natural convection of an electrically conducting fluid in a square differentially heated cavity using the control volumes method. An inclined external magnetic field is considered with Pr=0.733, Ra/Pr=10^6, 0≤Ha≤100, different field inclinations. Authors concluded that at high Ha values velocities are damped and the convective heat transfer rate is reduced. The peak values of the total heat transfer appear in the low region of tilting angle rather than in the high region, once the magnetic field is applied. Once the magnetic field has been applied, the maximum values of the Nusselt number appear in the lower region of the inclination angle.

Gelfgat and Bar-Yoseph [19] studied the onset of oscillatory instability in convective flow in a slender cavity of Ar=4 filled by conducting fluid of Pr=0.015 associated with the horizontal Bridgman crystal growth process under imposed constant uniform magnetic field and using a spectral method (Global Galerkin method). Stability diagrams for steady single-cell and two cells flows showing the dependence of the critical Grashof number Gr_{cr} on Ha number and the magnetic field tilting angle are established. It has been concluded that a vertical magnetic field provides the strongest stabilization effect, multiplicity of steady states is suppressed and the single-cell flow remains stable to a certain range of Ha. The single-cell flows are destabilized after by increasing the Ha number.

2. Problem Statement

The problem under investigation is a two-dimensional rectangular enclosure of height the unit and width Ar=W/H filled with a viscous, incompressible and electrically conducting fluid. A temperature gradient $\Delta T=T_h-T_c$ is applied between vertical walls and is responsible of the convective onset and motion. The horizontal cavity walls are supposed to be insulated. The four walls are considered rigid and no-slip boundary condition is used for the velocity field. The fluid is permeated by a uniform horizontal magnetic field of strength B (Figure 1). The gravity field reigns in the vertical descendant direction. Induced magnetic field can be neglected in comparison with the imposed magnetic field.

The fluid properties are assumed to be constant, except the density taken as linear temperature-dependent: $\rho=\rho_0\left(1-\beta(T-T_c)\right)$.
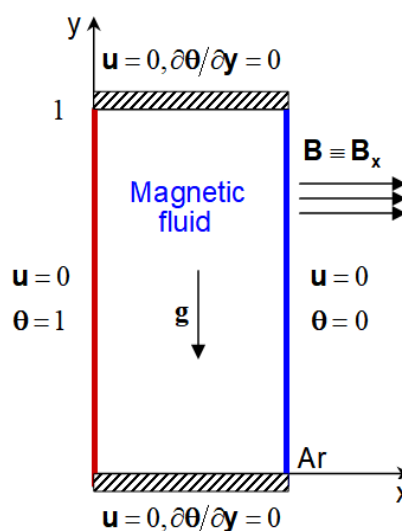

Fig. 1. Sketch of the problem

2.1. Governing Equations in Dimensionless Form

Neglecting viscous heat dissipation and compression work done by the pressure, the unsteady state governing equations can be summarized in the incompressible form as follows:

Continuity:
$$\nabla.U = 0 \tag{1}$$

Momentum:
$$\partial_t U + (U.\nabla)U = -\nabla P + \nabla.(\upsilon \nabla U) + \rho F / \rho_0 \tag{2}$$

Energy:
$$\partial_t T + (U.\nabla)T = \nabla.(\alpha \nabla T) \tag{3}$$

Where $F_i = \beta(T - T_\infty)g\delta_{i2} + \sigma[(B_j U_j)B_i - B^2 U_i]$ and B_j denotes the magnetic fields components $B_x = B$ and $B_y = 0$. We assume the Joule heating can be neglected since $Ra > 10^3$ and $Ha < 200$.

The flow is characterized by the Rayleigh number ($10^3 \le Ra \le 10^6$), the Prandtl number ($0.01 \le Pr \le 0.1$)), the Hartmann number ($0 \le Ha \le 150$) defined as:

$$Ra = g\beta\Delta T H^3 / \nu\alpha, Pr = \frac{\nu}{\alpha} \text{ and } Ha = H B\sqrt{\sigma/\mu} \tag{4}$$

The following changes of variables are implemented in the following:

$$\tau = \frac{t}{H^2/\alpha}, (x,y) = \frac{(X,Y)}{H}, (u,v) = \frac{(U,V)}{\alpha/H}, p = \frac{H^2 P}{\rho\alpha^2}, \theta = \frac{T - T_c}{T_h - T_c} \tag{5}$$

Dimensionless governing equations can be expressed accordingly as follows:

Continuity
$$\frac{\partial u}{\partial x} + \frac{\partial u}{\partial y} = 0 \tag{6}$$

Momentum
$$\frac{\partial u}{\partial \tau} + u\frac{\partial u}{\partial x} + v\frac{\partial u}{\partial y} = -\frac{\partial p}{\partial x} + Pr(\frac{\partial^2 u}{\partial x^2} + \frac{\partial^2 u}{\partial y^2})$$
$$\frac{\partial v}{\partial \tau} + u\frac{\partial v}{\partial x} + v\frac{\partial v}{\partial y} = -\frac{\partial p}{\partial y} + Pr(\frac{\partial^2 v}{\partial x^2} + \frac{\partial^2 v}{\partial y^2}) - Pr Ha^2 v + Ra Pr \theta \tag{7}$$

Energy
$$\frac{\partial \theta}{\partial \tau} + u\frac{\partial \theta}{\partial x} + v\frac{\partial \theta}{\partial y} = \frac{\partial^2 \theta}{\partial x^2} + \frac{\partial^2 \theta}{\partial y^2} \tag{8}$$

The boundary conditions used in the present problem are:

$$u(x,0) = u(x,1) = u(0,y) = u(1,y) = 0,$$
$$v(x,0) = v(x,1) = v(0,y) = v(1,y) = 0,$$
$$\partial_y \theta(x,0) = \partial_y \theta(x,1) = \theta(1,y) = 0, \ \theta(0,y) = 1.$$
(9)

The average Nusselt number along the hot wall is computed as:

$$Nu_0 = -\int_0^1 \left[\frac{\partial \theta}{\partial x} \right]_{x=0} dy = \sum_j (3\theta_{0,j} - 4\theta_{1,j} + \theta_{2,j})/2$$
(10)

The convergence criterion for steady state is defined as follows:

$$\left| \frac{\overline{Nu}(t+5000\Delta t) - \overline{Nu}(t)}{\overline{Nu}(t)} \right| \leq 10^{-4}$$
(11)

2.2. Computational Method

The lattice Boltzmann method is used for simulating the present fluid flow and heat transfer problem. The essence of using the double population distribution functions D2Q9-D2Q4 (Figure 2) is for its stability compared to the D2Q9-D2Q9 thermal model and it preserves the computational efforts, since the collision step takes around 70% of the CPU time. The evolution of the distribution functions in the D2Q9-D2Q4 lattice model in the presence of source term S_k is written as:

$$f_k(\boldsymbol{x} + \boldsymbol{e}_k \Delta t, t + \Delta t) = f_k(\boldsymbol{x},t) - \frac{1}{\tau_v} \left(f_k(\boldsymbol{x},t) - f_k^{eq}(\boldsymbol{x},t) \right) + \Delta t \, F_k, \quad k = 0-8$$
(12)

And

$$h_k(\boldsymbol{x} + \boldsymbol{e}_k \Delta t, t + \Delta t) = h_k(\boldsymbol{x},t) - \frac{1}{\tau_\alpha} \left(h_k(\boldsymbol{x},t) - h_k^{eq}(\boldsymbol{x},t) \right), \qquad k = 1-4$$
(13)

In the present study, an acceleration technique originally proposed by Guo et. (2004) [20] and was used in our previous works to solve flows with body force and was found to be very efficient, offers more stability, allows accurate results for coarser grid-size and speeds-up the convergence for steady flows or the established regime for unsteady flows. The model is quite simple compared to others acceleration techniques such as Multi-Grid technique.

The correspondent equilibrium parts f_k^{eq} and g_k^{eq} are modifed as:

$$f_k^{eq}(\boldsymbol{x},t) = \omega_k \rho \left(1 + \frac{\boldsymbol{e}_k . \boldsymbol{u}}{c_s^2} + \frac{(\boldsymbol{e}_k . \boldsymbol{u})^2 - c_s^2 \boldsymbol{u}^2}{2\zeta c_s^4}\right), \ g_k^{eq}(\boldsymbol{x},t) = \varpi_k \rho \theta \left(1 + \frac{\boldsymbol{e}_k . \boldsymbol{u}}{\bar{\zeta} \bar{c}_s^2}\right)$$
(14)

Where $\varpi_{k=1-4} = 1/4$, $c_s^2 = 1/3$ for the D2Q9 dynamic model and $\bar{c}_s^2 = 1/2$ for the D2Q4 thermal model. The factors ζ and $\bar{\zeta}$ are the accelerating factors ranging in [0,1] and taken here 0.1 and ω_k are weighting factors and $\boldsymbol{e}_k$ are the lattice velocity vectors. For the D2Q9 LB model we have:

$$\begin{pmatrix} \omega_k \\ e_{k,x} \\ e_{k,y} \end{pmatrix} = \begin{pmatrix} \frac{4}{9}, \frac{1}{9}, \frac{1}{9}, \frac{1}{9}, \frac{1}{9}, \frac{1}{36}, \frac{1}{36}, \frac{1}{36}, \frac{1}{36} \\ 0, 1, 0, -1, 0, 1, -1, -1, 1 \\ 0, 0, 1, 0, -1, 1, 1, -1, -1 \end{pmatrix} \tag{15}$$

The forcing term S_k allowing absorption of the artefact due to the lattice effect according to Guo *et al.,* [21] and accounting for the accelerating modification is chosen here:

$$F_k = \omega_k f_k^{eq} \frac{\boldsymbol{e}_k}{\zeta c_s^2}.\boldsymbol{F} \tag{16}$$

The modified SRTs τ_υ and τ_α appearing in Eq. (12-13) are linked to the kinematic viscosity and thermal diffusivity as:

$$\frac{\upsilon}{\zeta} = \frac{2\tau_\upsilon - 1}{6} \frac{\Delta x^2}{\Delta t} , \quad \frac{\alpha}{\bar{\bar{\zeta}}} = \frac{2\tau_\alpha - 1}{4} \frac{\Delta x^2}{\Delta t} \tag{17}$$
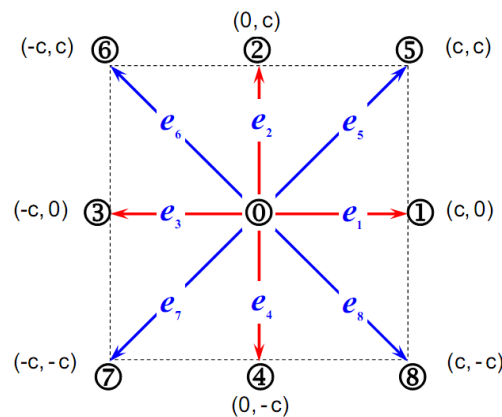

Fig. 2. The nine-particle speeds model used in the hydrodynamic of lattice Boltzmann equation. Only the four red velocities are necessary for the temperature field

In LB heat and flow modeling philosophy, the macroscopic variables: density, velocity and temperature are computed as:

$$\left[\rho(x,t),\, \rho\boldsymbol{u}(x,t),\, \theta(x,t)\right] = \sum \left[f_{k=0-8}^{eq},\, \boldsymbol{e}_k f_{k=0-8}^{eq},\, h_{k=1-4}^{eq} \right] \tag{18}$$

Since it affects the accuracy of the computations, implementation of boundaries conditions is a very important issue in LBM. The second-order bounce back boundary rule for the non-equilibrium distribution function proposed by Zou and He (1997) [22] is used to account for the no-slip boundary condition along the four walls as:

$$\left(f - f^{eq}\right)^{in} = \left(f - f^{eq}\right)^{out} \tag{19}$$

Where the asterisk "in" and "out" denote for inner (unknown) and outer (known) particles respectively at the wall node:

$$f_\alpha = \left(f_\beta - f_\beta^{eq} \right) + f_\alpha^{eq} \qquad (20)$$

Where $\alpha = 2,5,7$: at $y=0$, $\alpha = 4,7,8$: at $y=1$, $\alpha = 1,5,8$: at $x=0$ and $\alpha = 3,6,7$: at $x=1$. For the temperature field, the temperature distribution functions at the isothermal walls obey to the condition: $h_\alpha^{in} = -h_\alpha^{out} + (\varpi_\alpha + \varpi_\beta)\theta_{wall}$. However, the adiabatic boundary condition is transferred to Dirichlet-type condition using the conventional second-order finite difference approximation as: $g_{wall} = (4 g_{wall \pm \Delta y} - g_{wall \pm 2\Delta y})/3$, which can be summarized as follows:

$$
\begin{aligned}
&h_1(0,y) = -h_3(0,y) + (v_1 + v_3).\theta_c : \quad at\ x = 0,\\
&h_3(1,y) = -h_1(1,y) + (v_1 + v_3).\theta_h : \quad at\ x = 1,\\
&h_2(x,0) = \left[4h_2(x,\Delta y) - h_2(x,2\Delta y) \right]/3 : at\ y = 0,\\
&h_4(x,1) = \left[4h_4(x,1-\Delta y) - h_4(x,1-2\Delta y) \right]/3 : at\ y = 1.
\end{aligned}
\qquad (21)
$$

2.3. Benchmarking the LB Thermal Model

To ensure the current code correctness and accuracy, two test cases are used for problems evolving MHD effects, different Prandtl numbers and solution methods. The average Nusselt numbers along with the hot wall are used for comparison and are presented in Table 1 as well as reference results using different numerical approaches.

In the present validation, are used for comparison the FEM results emerging from the FEM Comsol Multiphysics [23] using 10170 triangular elements with refinement near walls. As one can remark, an excellent agreement between the present calculations based on LBM and FEM is obtained. The corresponding average deviation is close to 1.072%. The present results are in good agreement with the results of references [13, 15, 16] using the LBM, FEM, FDM and the spectral GDQ approaches respectively.

The computations of Rudraiah [24] are found to be non-accurate at high Ha numbers, as well as the results of reference [13, 24, 25] which show clear deviations compared to the benchmark general tendency. Notice that Lo [26] results are obtained using a high-resolutions scheme. The maximum deviations of the computed Nusselt numbers between current results and Lo [26] are found to be within 0.14% and 0.97% for the FEM and LBM approaches respectively,

Table 1
Comparison of the present LBM and FEM results with referenced results using different approaches for different Grashof numbers (Gr = Ra/Pr) and Hartmann numbers at Pr = 0.733

References		[13]	[14]	[15]	[16]	[24]	[25]	[26]	Present	
		Numerical appoach								
Ra/Pr	Ha	LBM	FVM	FEM	FDM	FDM	FVM	GDQ	FEM	LBM
2×10^4	0	-	-	2.5439	2.5308	2.5188	2.6237	2.5303	2.5308	2.5250
	10	2.2780	2.2976	2.2385	2.2383	2.2234	2.3234	2.2381	2.2382	2.2343
	50	1.0900	1.1154	-	1.0761	1.0856	1.0987	1.0756	1.0761	1.0780
	100	1.0177	1.0113	1.0066	1.0062	1.0110	1.0245	1.0048	1.0062	1.0091
2×10^5	0	-	-	5.0245	5.0795	4.9198	5.1876	5.0814	5.0814	5.0577
	10	5.0518	4.9865	4.9136	4.9712	4.8053	4.9825	4.9752	4.9730	4.9420

	50	3.0784	3.2901	-	2.9942	2.8442	2.9784	2.9966	2.9948	2.9929
	100	1.4866	1.6430	1.4292	1.4629	1.4317	1.6318	1.4644	1.4628	1.4786
2×10^6	0	-	-	-	-	8.7030	-	-	9.8484	9.7044
	10	9.8852	9,7904	-	-	8.6463	-	-	9.8051	9.7229
	50	8.9326	9.0563	-	-	7.5825	-	-	8.829	8.7666
	100	6.7142	7.2416	-	-	5.5415	-	-	6.5869	6.5965

It shall be noted here, that the most doubtful results are obtained for Ra/Pr=2×10^6. For this reason, we use the theory of Richardson extrapolation (TRE) to obtain grid independent solution for this Ra value. Three non-uniform structural quadrangular grids are used 20×20, 40×40 and 80×80 with geometrical symmetric distribution and elements aspect ratio of four (04) as shown in Figure 3. We denote Nu_m, Nu_{2m} and Nu_{4m} the Nusselt number values for edge elements number 20, 40 and 80. In the TRE, the order of the scheme and the discretization error are computed as:

$$\delta = \frac{log\,\dfrac{\Delta Nu_{2m\text{-}m}}{\Delta Nu_{4m\text{-}2m}}}{log(2)}\,,\; \varepsilon_{4m}^d \approx \frac{\Delta Nu_{4m\text{-}2m}}{2^\delta - 1} \tag{22}$$

Where $\Delta Nu_{2m\text{-}m} = Nu_{2m} - Nu_m$ and the 2 refers to the increase in mesh refinement.

In the TRE, the grid independent solution is obtain as: $Nu = Nu_{4m} + \varepsilon_{4m}^d$. For the case Ha=100 the obtained values are δ = 2.26065 and ε_{4m}^d =-0.00533 and thus Nu (Ha=100)= 6.57387. Are found also Nu (Ha=0)= 9.83178, Nu(Ha=10)= 9.78841 and Nu(Ha=50)= 8.81225. More refinement using elements numer of 120 gives Nu values 9.8347, 9.7914, 8.8154 6.5768 which are within less than 0.044% close to the estimate grid independent solution. These values are within less than 0.2% deviation compared to our FEM results presented in Table 1 and within less than 1.3% compared to our LBM results, which reinforces the high accuracy of the present LBM model.
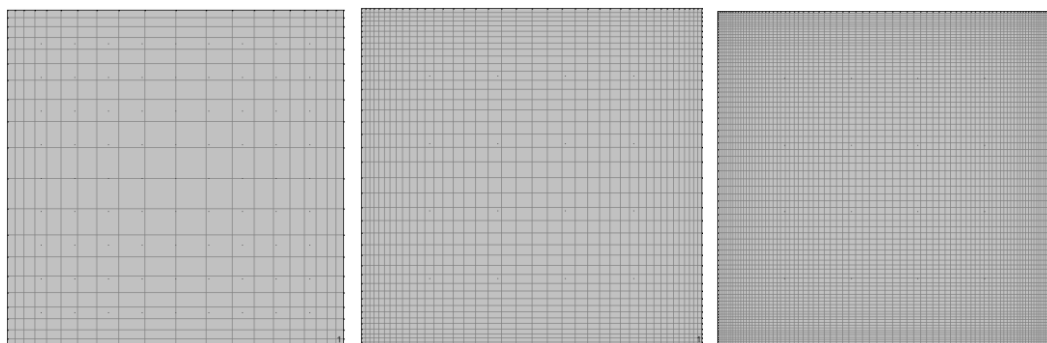

Fig. 3. Mesh structures for edge elements number 20, 40 and 80

The second test case concerns the simulations of natural convection in square cavity filled with a low Prandtl number fluid (Pr=0.025) for Ra ranging from 10^4 to 10^6. The plots of u_{max}/Ra and v_{max}/Ra vs Ha in Log-Log scales are shown in Figure 4. The fitting curves are the correlations established by Yu *et al.,* [16]. Not that in Yu *et al.,* plots, only the envelope curves as asymptotic behavior are fitted and plotted without accounting for low Ha effects at each Ra number as depicted in the Figure 4.
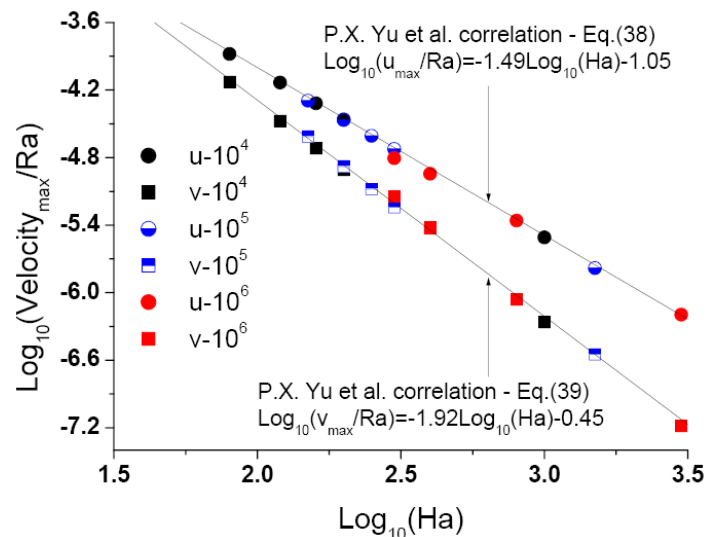
Fig. 4. Plots of u_{max}/Ra and v_{max}/Ra vs Ha in Log-Log scales with fitted curves provided by Yu *et al.,* [16] for Pr=0.025 and Ra ranging from 10^4 to 10^6

3. Results

In the following parts, the stability behaviour inside the tall cavities will be presented and discussed as a consequence of the Prandtl (Pr=0.01, 0.1) number variation as well as the aspect ratio Ar=W/H (Ar=1/8, 1/4, 1/2). In each figure, for a given Rayleigh number value of the considered flow conditions (Pr, Ar), a Hartmann number value is sought beyond which flow unsteadiness is absent, and such value is called critical and noted Ha_{cr}.

3.1. Behaviour of Marginal Stability Curves: Ha_{cr}= f(Ra, Ar, Pr=0.01)
3.1.1. Case with Ar=1/2

Figure 5 depicts the variation of the critical Hartman number as a function of the Rayleigh number for Ar=0.5 and Pr=0.01. The dynamic and thermal structures for some simulated points are gathered to the transition thresholds curve. For low Rayleigh numbers the dynamic structure is a large elliptic cell with two attached small cells to the first bisector and two others detached cells at the second bisector. The critical Hartmann number is nearly a linear function of the Rayleigh number for Ra≤10^5, however the tendency becomes like parabolic to Ra=10^6. The isotherms are vertical lines near the cavity floor and ceiling and are clockwise distorted near the cavity centre.

Increasing the Rayleigh number, the big cell becomes more and more enlarged. At Ra=10^6, the cavity is occupied by one y-elongated big cell with six small cells centro-symmetric along the second bisector. The thermal layers along more weakened to the active walls.

For benchmarking purpose of the values of plotted points are summarized in Table 2. Calculated values of the Nusselt number and the maximum and minimum stream-function values are also given for some Ra where the dynamic and thermal structures distributions are plotted in Figure 5.
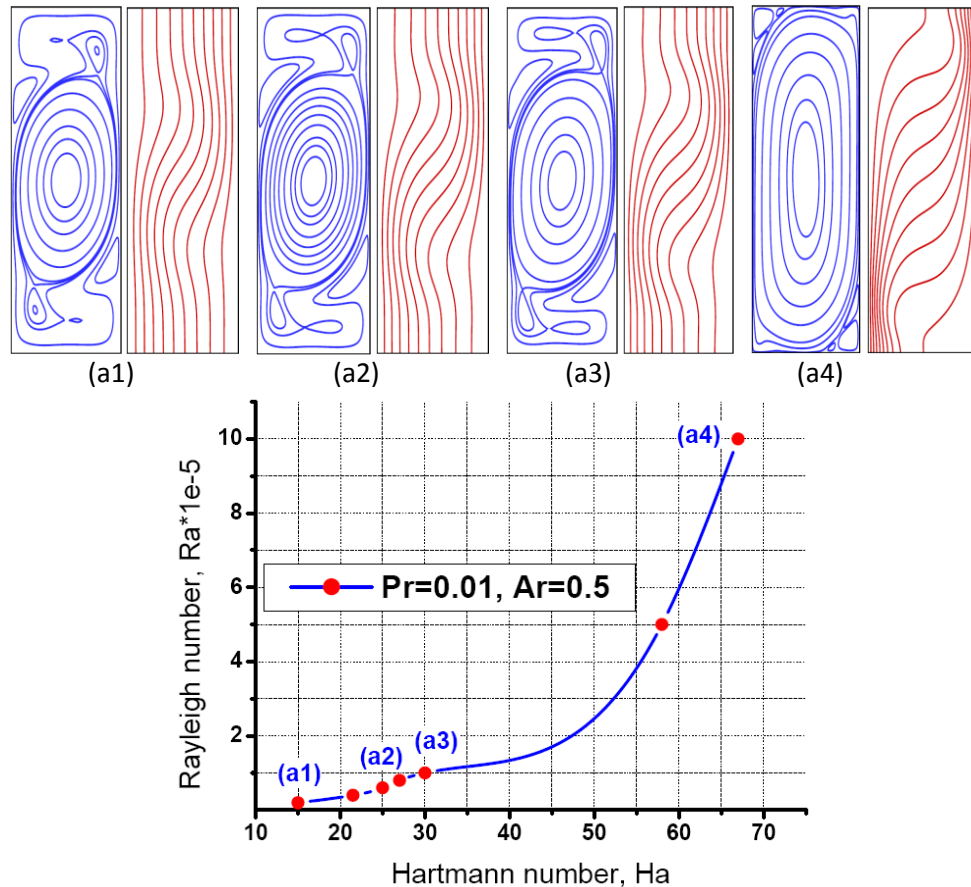
(a1)   (a2)   (a3)   (a4)

Fig. 5. Transition thresholds to convective unsteadiness under horizontal magnetic for Pr=0.01 and Ar=0.5

Table 2

Critical Hartmann number Ha_{cr} as a function of the Rayleigh number Ra: Case with Pr=0.01, Ar=0.5.

$Ra/10^5$	0.2	0.4	0.6	0.8	1.0	5.0	10
Ha_{cr}	15	21.5	25	27	30	58	67
Nu	2.320	-	2.615	-	2.845	-	5.025
Ψ_{max}	0.011	-	0.0244	-	0.0342	-	0.009
Ψ_{min}	-2.376	-	-3.173	-	-3.727	-	-6.713

3.1.2. Case with Ar=1/4

The stability curve $Ha_{cr}=f(Ra)$ for Pr=0.01 and Ar=0.25 is shown in Figure 6 gathered with the dynamic and thermal structures of four selected threshold points. At low Rayleigh number Ra=8×10⁴, the critical Hartmann number is close to 17. The flow at low Prandtl numbers is know to be very instable at least for the very interesting cases of horizontal and vertical Bridgman cavities filled with liquid Gallium at Pr=0.015 [11,14,17]. In this case of study, the dynamic and thermal structures are exactly doubled in the y-direction as the cavity hight is doubled too.

By increasing the Rayleigh number, the thermal convection currents are enhanced and consequently the fluid distribution inside the rectangular domain seeks for more stably structures with reduced stresses and frictions. The flow becomes three clockwise rotating cells with a big and like elliptic one at the cavity centre slightly tilted to the right. The volume of both small cells decreases in favour of the central cell one. At high Rayleigh number (Ra=2×10⁶) the central cell is

more elongated vertically. This is mainly due to the competition between the buoyancy force and the magnetic force in the y-direction:

$$F_b = Ra \times \Pr \times \theta \ and \ F_m = -Ha^2 \times \Pr \times V \qquad (23)$$

Consequently, as the buoyancy force rises by increasing the Rayleigh number, as the magnetic force is enhanced in the opposite sense which leads to a stretching phenomenon of the large cell. The values of plotted points are summarized in Table 3.
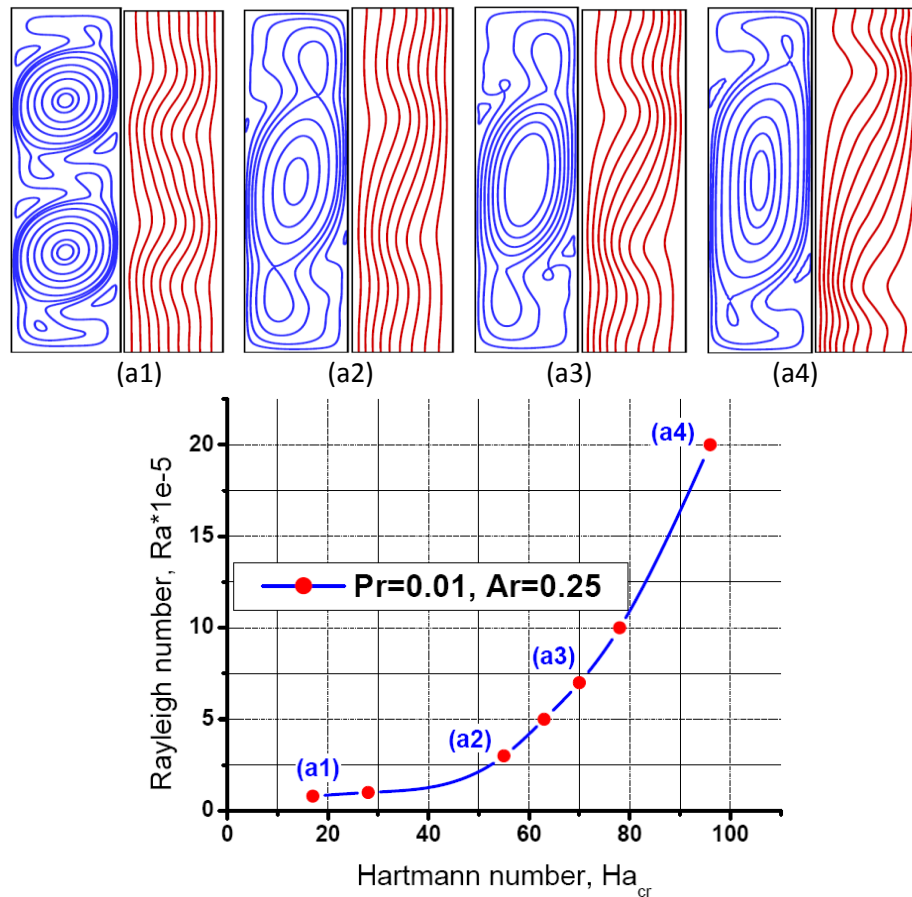

Fig. 6. Transition thresholds to convective unsteadiness under horizontal magnetic for Pr=0.01 and Ar=0.25

Table 3
Critical Hartmann number Ha_{cr} as a function of the Rayleigh number Ra: Case with Pr=0.01, Ar=0.25

$Ra/10^5$	0.8	1	3	5	7	10	20
Ha_{cr}	17	28	55	63	70	78	96
Nu	4.347	-	4.329	-	4.716	-	5.515
Ψ_{max}	0.089	-	0	-	0.006	-	0.550
Ψ_{min}	-1.729	-	-2.465	-	-3.584	-	-5.355

3.1.3. Case with Ar=1/8

Figure 7 presents the dynamic and thermal structures as well as the stability curve of the Hartmann number as a function of the Rayleigh number. Because of the elongation of the cavity vertically, the flow becomes more and more unstable.

In this condition Ar = 0.125, the dynamic structure is a four equal big rotating cells. The behaviour for Ar=0.25 is exactly doubled in the case Ar=0.125. Increasing more the Ra number, the streamlines form a three cells structure and the isotherms become more and more distorted to form sinusoids. At high Rayleigh numbers, the three cells are completely detached. The values of plotted points are summarized in Table 4 as well as the corresponding Nusselt number and minimum and maximum stream-function predicted values. It is worth to mention here that even the flow is stabilized and the currents are dumped, the heat transfer is augmented.
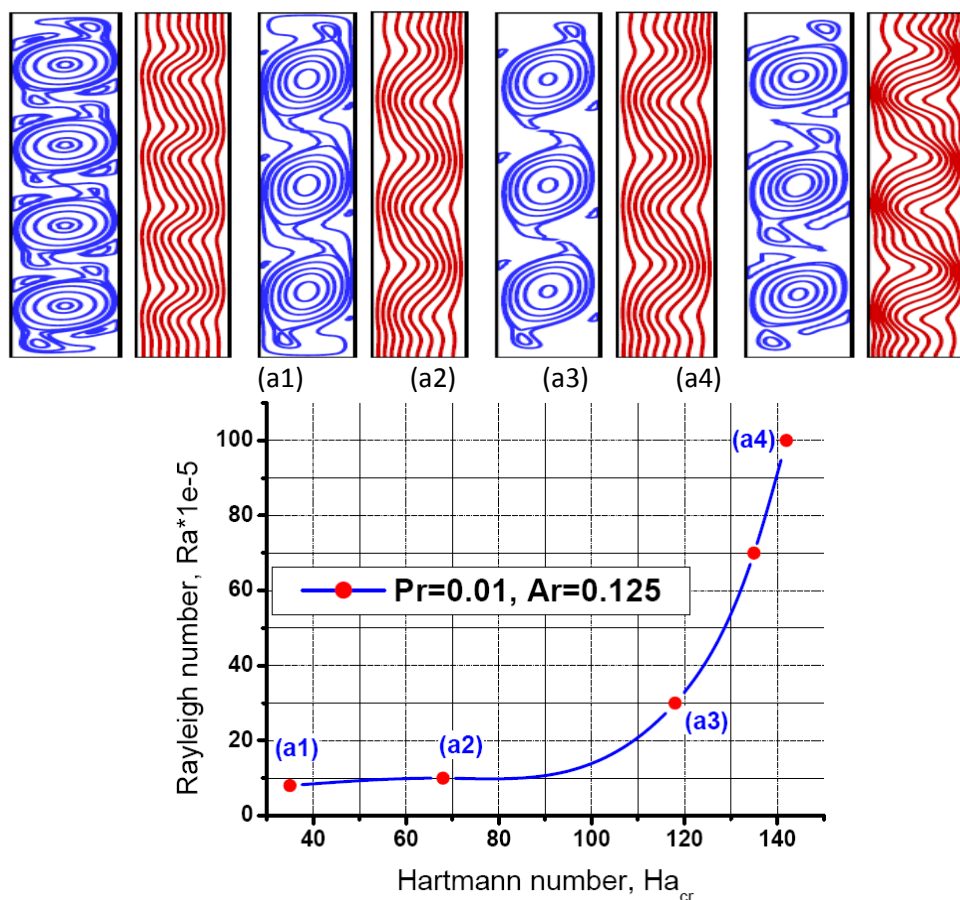

Fig. 7. Transition thresholds to convective unsteadiness under horizontal magnetic for Pr=0.01 and Ar=0.125

Table 4
Critical Hartmann number Ha_{cr} as a function of the Rayleigh number Ra: Case with Pr=0.01, Ar=0.125

$Ra/10^5$	8	10	30	70	100
Ha_{cr}	35	67	118	133	143
Nu	8.814	8.545	9.072	-	11.663
Ψ_{max}	0.0255	0.0124	0.0045	-	0.0901
Ψ_{min}	-1.959	-1.950	-2.605	-	-4.641

3.2. Behaviour of the Marginal Stability Curves: $Ha_{cr}= f(Ra, Ar, Pr=0.1)$
3.2.1. Case with Ar=1/2

By increasing the Prandtl number from 0.01 to 0.1 with Ar=0.5, the flow dynamic structure is a large cell occupying the whole domain with two small detached clockwise rotating cells in its centre. To stabilize the flow, the rise in the Ha number is more acute as the rise in the Ra number until Ra≈10^6. In fact, the buoyancy force acts near the hot and cold walls where thin boundary layers are phenomenon holds. The centre remains, however, as a low activity recirculation zone which is transformed into an activity zone of the magnetic field in its vertical circumferential side.

This is well marked in Figure 8 (a2) where the cell from above has a tail down in the direction of action of the magnetic force; and that from below has a tail stretched upwards in the direction of action of the magnetic force opposed to the y-velocity. The values of plotted points are summarized in Table 5 as well as the corresponding Nusselt number and minimum and maximum stream-function predicted values

The counter-acting (stretching) effect between the magnetic and buoyancy forces at the cavity core becomes pronounced beyond Ra=20×10^5 to Ra=10^7 where several cells appear and a clear vertical thermal stratification holds.

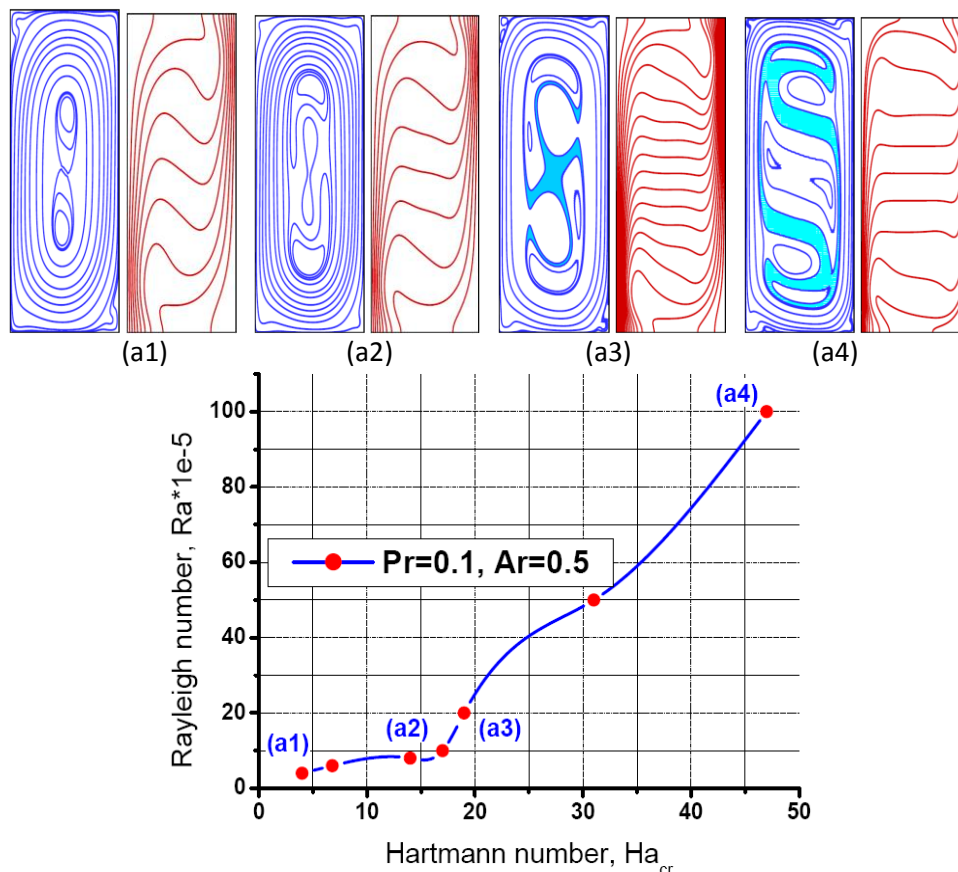The heat transfer as a function of the Rayleigh number obey approximately the law Nu=0.3766×$Ra^{0.2229}$.

Fig. 8. Transition thresholds to convective unsteadiness under horizontal magnetic for Pr=0.1 and Ar=0.5

Table 5
Critical Hartmann number Ha_{cr} as a function of the Rayleigh number Ra: Case with Pr=0.1, Ar=0.5

$Ra/10^5$	4	6	8	10	20	50	100
Ha_{cr}	4	6.8	14	17	19	31	45.5
Nu	6.693	-	7.728	-	9.632	-	13.650
Ψ_{max}	0.0083	-	0.0129	-	0.0173	-	0.0545
Ψ_{min}	-12.767	-	-12.657	-	-14.953	-	-19.130

3.2.2. Case with Ar=1/4

In this case the flow is three rotating cells at low Ra number with elliptic big cell tilted to the first bisector (Figure 9). Increasing the Ra number to 5×10^6, a main like rectangular cell occupies the whole domain with two very small attached cells along the second bisector. As explained here-above, as the Rayleigh number is increased, the critical Hartmann number is increased accordingly. However, for high values of the last, the effects on the dynamic and thermal structures are significant leading to the S-structure at the cavity core and to a thermal vertical stratification. For Ra=10^7, the flow is a single cell and the thermal boundary layers are more stretched to the active hot and cold walls due to the enhanced buoyancy. The values of plotted points are summarized in Table 6 as well as the corresponding Nusselt number and minimum and maximum stream-function predicted values

The critical Ha number interpolation as a function of the Ra number leads to best fitted curve of polynomial model: $Ha_{cr}=12.9249+0.6751\times Ra'-1.8924\times10^{-3}*Ra'^2$ with $Ra'=Ra/10^5$, a standard error close to 0.3353 and a correlation coefficient close to 0.9999.
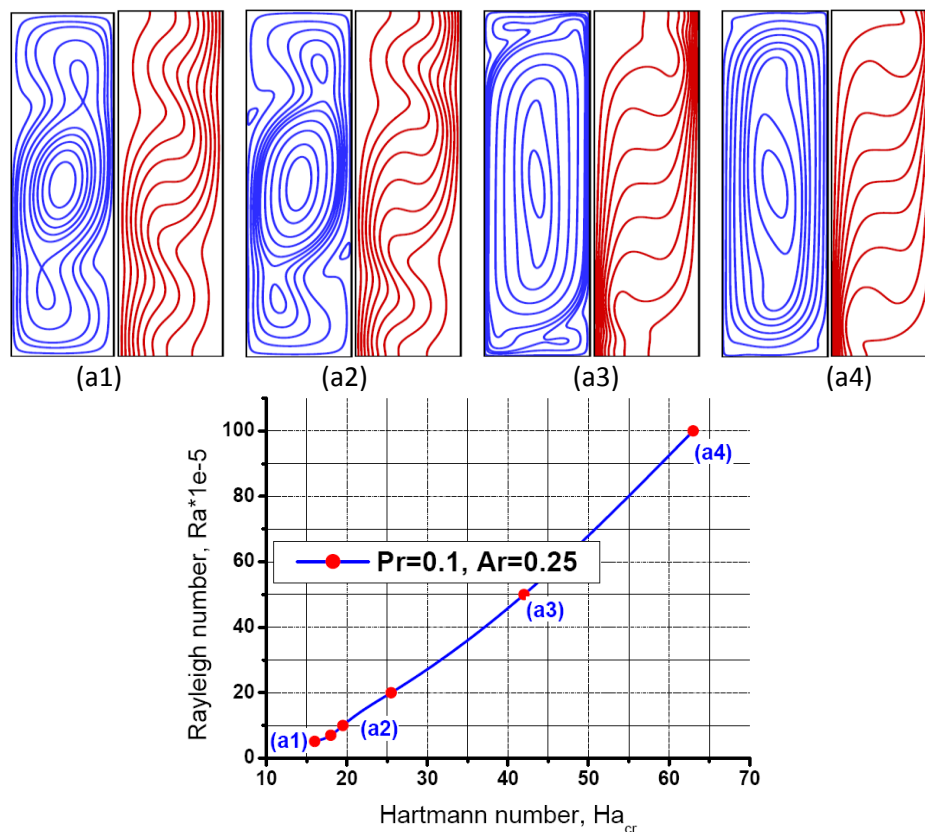

Fig. 9. Transition thresholds to convective unsteadiness under horizontal magnetic for Pr=0.1 and Ar=0.25

Table 6
Critical Hartmann number Ha_{cr} as a function of the
Rayleigh number Ra: Case with Pr=0.1, Ar=0.25

$Ra/10^5$	5.12	7	10	20	50	100
Ha_{cr}	16	18	19.5	25.5	42	61.5
Nu	6.252	-	7.335	-	11.552	13.565
Ψ_{max}	0.0046	-	0.0163	-	0.0171	0.0192
Ψ_{min}	-9.701	-	-12.595	-	-17.383	-18.952

3.2.3. Case with Ar=1/8

The case with Ar=0.125, shows three elliptic attached cells with eight small eddies near $Ra=10^7$ (Figure 10). The thermal structure is clearly deformed. The small cells disappear gradually with Ra rise. Beyond Ra = 3×10^7 to 5×10^7, the middle cell becomes elongated and the flow remains three cells. The instability seems to be more pronounced with Pr=0.01 compared to that with Pr=0.1. In fact, for Ra=5×10^7 a Ha=103 value is sufficient to suppress the unsteadiness behaviour. However for Pr=0.01, Ha=143 is necessary to stabilize the flow under Ra=10^7. This is attributed to the large density (inducing inertia currents) and heat capacity such as mercury and Gallium. The values of plotted points are summarized in Table 7 as well as the corresponding Nusselt number and minimum and maximum stream-function predicted values.
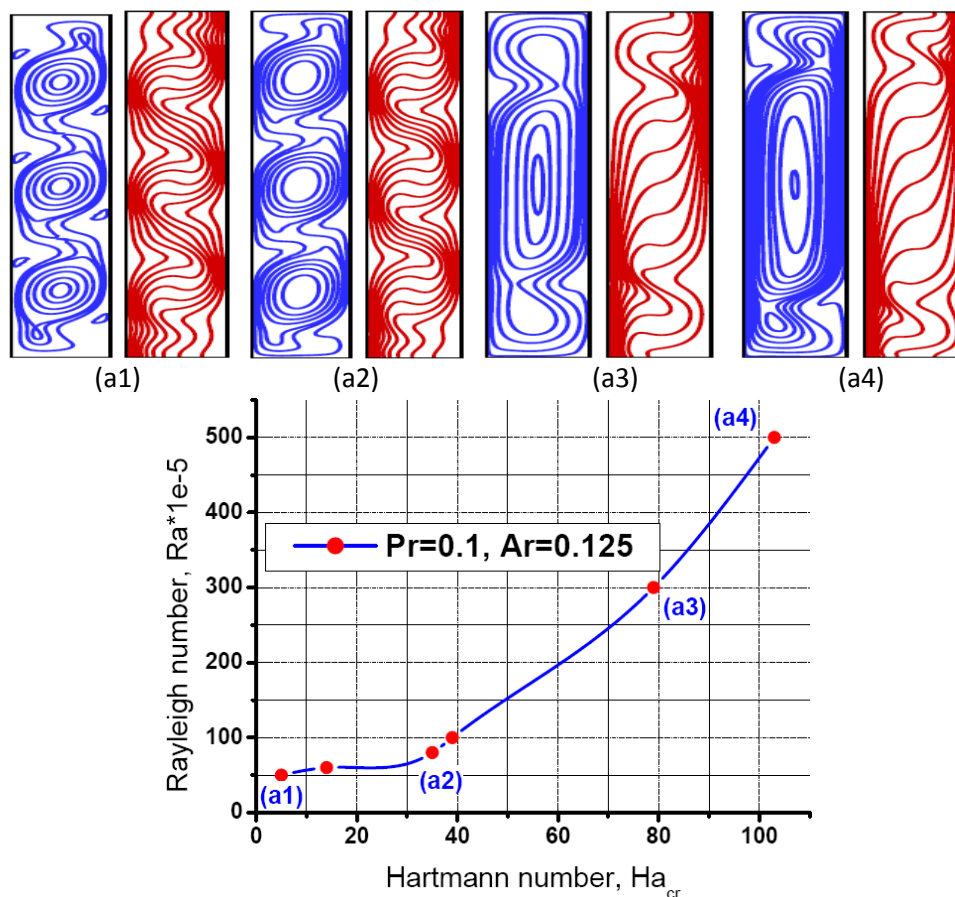

Fig. 10. Transition thresholds to convective unsteadiness under horizontal magnetic for Pr=0.1 and Ar=0.125

Table 7
Critical Hartmann number Ha_{cr} as a function of the Rayleigh number Ra: Case with Pr=0.1, Ar=0.125

$Ra/10^5$	50	60	80	100	300	500
Ha_{cr}	5	14	35	39	79	103
Nu	13.541	-	15.230	-	17.807	19.273
Ψ_{max}	0.0274	-	0.0094	-	0.0209	0.0375
Ψ_{min}	-10.665	-	-11.653	-	-24.475	-26.482

4. Conclusions

Routes to oscillations instability behavior inside tall cavities is investigated numerically at low Prandtl numbers (Pr=0.01- 0.1) under externally imposed horizontal uniform magnetic field for a wide ranges of Ra, Ha numbers and aspect ratio. The LBM approach is used to solve the PD governing equations. The onset of convective motion and heat transfer arise from a horizontal temperature gradient. Analysis of flow and thermal behaviours and the heat transfer rate along with the active walls are carried out. It has been concluded throughout this study the following conclusions:

I. The flow at Pr=0.01 typical of liquid metal is strongly unstable and presents multi-cellular structure compared to Pr=0.1 cases.
II. The flow oscillatory instability is enhanced by decreasing the cavity aspect ratio Ar.
III. The Magnetic field magnitude necessary to stabilize the flow is the weaker for Pr=0.1.
IV. The flow undergoes transition to steady state with fewer cells at high Ra and the transition occurs at a threshold value showing weak growth rate in the Ha_{cr} compared to Ra variation.
V. Increasing the Prandtl number to 0.1, the core flow structure is distorted due to the Lorentz forces which outweigh the buoyancy forces and a thermal stratification is clearly established.
VI. At high Ha numbers and Rayleigh numbers, the stretching effects suppress the unsteady behaviour and results in steady state with extended unicellular pattern in the direction of Lorentz force.

The LBM approach is found to be a powerful tool to deal with problems focusing on the accuracy to identify transitional thresholds at low Prandtl number fluids where major endeavours are mainly focusing of steady or fully unsteady solution flows.

References
[1]   Okada, K., and H. Ozoe. "Experimental heat transfer rates of natural convection of molten gallium suppressed under an external magnetic field in either the X, Y, or Z direction." *Journal of Heat Transfer* 114, no. 1 (1992): 107-114.
[2]   Surek, T., B. Chalmers, and A. I. Mlavsky. "The edge-defined film-fed growth of controlled shape crystals." *Journal of Crystal Growth* 42 (1977): 453-465.
[3]   HADID, HAMDA BEN, and Daniel Henry. "Numerical study of convection in the horizontal Bridgman configuration under the action of a constant magnetic field. Part 2. Three-dimensional flow." *Journal of Fluid Mechanics* 333 (1997): 57-83.
[4]   Zhou, Hong, and A. Zebib. "Oscillatory convection in solidifying pure metals." *Numerical Heat Transfer* 22, no. 4 (1992): 435-468.
[5]   Larroude, P. H., J. L. I. D. Ouazzani, J. I. D. Alexander, and P. Bontoux. "Symmetry breaking flow transitions and oscillatory flows in a 2D directional solidification model." *European journal of mechanics. B, Fluids* 13, no. 3 (1994): 353-381.

[6]   Hurle, D. T. J., and R. W. Series. "Use of a magnetic field in melt growth." *Handbook of crystal growth* 2 (1994): 261-285.

[7]   DJEBALI, Ridha, Mohamed Ammar ABBASSI, and Ahlem ROUAHI. "Conjugate Effects of Buoyancy and Magnetic Field on Heat and Fluid Flow Pattern at Low-to-Moderate Prandtl Numbers" *International Letters of Chemistry, Physics and Astronomy*, 66 (2016): 79-95.

[8]   Nagasasikala, Madduleti, and Bommanna Lavanya. "Effects of Dissipation and Radiation on Heat Transfer Flow of a Convective Rotating Cuo-Water Nano-fluid in a Vertical Channel." *Journal of Advanced Research in Fluid Mechanics and Thermal Sciences* 50, no. 2 (2018): 108-117.

[9]   E. K. Ghiasi and R. Saleh; "Analytical and Numerical Solutions to the 2D Sakiad is Flow of Casson Fluid with Cross Diffusion, Inclined Magnetic Force, Viscous Dissipation and Thermal Radiation Based on Buongiorno's Mathematical Model"; *CFD Letters*, 11(1) (2018): 42-57.

[10]   Hurle, D. T. J. "Temperature oscillations in molten metals and their relationship to growth striae in melt-grown crystals." *The Philosophical Magazine: A Journal of Theoretical Experimental and Applied Physics* 13, no. 122 (1966): 305-310.

[11]   Djebali, Ridha, Habib Sammouda, and Mohammed El Ganaoui. "Some advances in applications of lattice Boltzmann method for complex thermal flows." *Adv. Appl. Math. Mech* 2, no. 5 (2010): 587-608.

[12]   Ece, Mehmet Cem, and Elif Büyük. "Natural-convection flow under a magnetic field in an inclined rectangular enclosure heated and cooled on adjacent walls." *Fluid Dynamics Research* 38, no. 8 (2006): 564.

[13]   Djebali, Ridha, Mohamed ElGanaoui, and Taoufik Naffouti. "A 2D Lattice Boltzmann full analysis of MHD convective heat transfer in saturated porous square enclosure." *Computer Modeling in Engineering and Sciences* 84, no. 6 (2012): 499.

[14]   Djebali, Ridha, Bernard Pateyron, and Mohamed El Ganaoui. "Prandtl Number Signature on Flow Patterns of Electrically Conducting Fluid in Square Enclosure." *Computer Modeling in Engineering & Sciences(CMES)* 88, no. 4 (2012): 293-307.

[15]   Sathiyamoorthy, M., and Ali J. Chamkha. "Natural convection flow under magnetic field in a square cavity for uniformly (or) linearly heated adjacent walls*." International Journal of Numerical Methods for Heat & Fluid Flow* 22, no. 5 (2012): 677-698.

[16]   Yu, P. X., J. X. Qiu, Q. Qin, and Zhen F. Tian. "Numerical investigation of natural convection in a rectangular cavity under different directions of uniform magnetic field." *International Journal of Heat and Mass Transfer* 67 (2013): 1131-1144.

[17]   El Ganaoui, Mohammed, and R. Djebali. "Aptitude of a lattice Boltzmann method for evaluating transitional thresholds for low Prandtl number flows in enclosures." *Comptes Rendus Mécanique* 338, no. 2 (2010): 85-96.

[18]   Han, Cho Young. "Effect of a magnetic field on natural convection of an electrically conducting fluid in a tilted cavity." *Journal of the Korean Physical Society* 55, no. 5 (2009): 2193-2199.

[19]   Gelfgat, A. Yu, and P. Z. Bar-Yoseph. "The effect of an external magnetic field on oscillatory instability of convective flows in a rectangular cavity." *Physics of Fluids* 13, no. 8 (2001): 2269-2278.

[20]   Guo, Zhaoli, T. S. Zhao, and Yong Shi. "Preconditioned lattice-Boltzmann method for steady flows." *Physical Review E* 70, no. 6 (2004): 066706.

[21]   Guo, Zhaoli, Chuguang Zheng, and Baochang Shi. "Discrete lattice effects on the forcing term in the lattice Boltzmann method." *Physical Review E* 65, no. 4 (2002): 046308.

[22]   Zou, Qisu, and Xiaoyi He. "On pressure and velocity boundary conditions for the lattice Boltzmann BGK model." *Physics of fluids* 9, no. 6 (1997): 1591-1598.

[23]   Comsol, A. B. "COMSOL Multiphysics reference manual." *Version* (2007).

[24]   Rudraiah, N., R. M. Barron, M. Venkatachalappa, and C. K. Subbaraya. "Effect of a magnetic field on free convection in a rectangular enclosure*." International Journal of Engineering Science* 33, no. 8 (1995): 1075-1084.

[25]   Kandaswamy, P., S. Malliga Sundari, and N. Nithyadevi. "Magnetoconvection in an enclosure with partially active vertical walls." *International Journal of Heat and Mass Transfer* 51, no. 7-8 (2008): 1946-1954.

[26]   Lo, D. C. "High-resolution simulations of magnetohydrodynamic free convection in an enclosure with a transverse magnetic field using a velocity–vorticity formulation." *International Communications in Heat and Mass Transfer* 37, no. 5 (2010): 514-523.